Electronic Supplementary Material (ESI) for Physical Chemistry Chemical Physics.
This journal is © the Owner Societies 2022

SUPPLEMENTARY INFORMATION for

Nanopore Facilitated Monohydrocalcitic Amorphous Calcium Carbonate Precipitation

Katharine Page,*[a,b], Andrew G. Stack,[c] Si Athena Chen[c] and Hsiu-Wen Wang*[c]

[a]Materials Science and Engineering Department, The University of Tennessee, Knoxville, TN 38996, USA.

[b]Neutron Scattering Division, Oak Ridge National Laboratory, Oak Ridge, TN 37831, USA.

[c]Chemical Sciences Division, Oak Ridge National Laboratory, Oak Ridge, TN 37831, USA.

1. Experimental setup

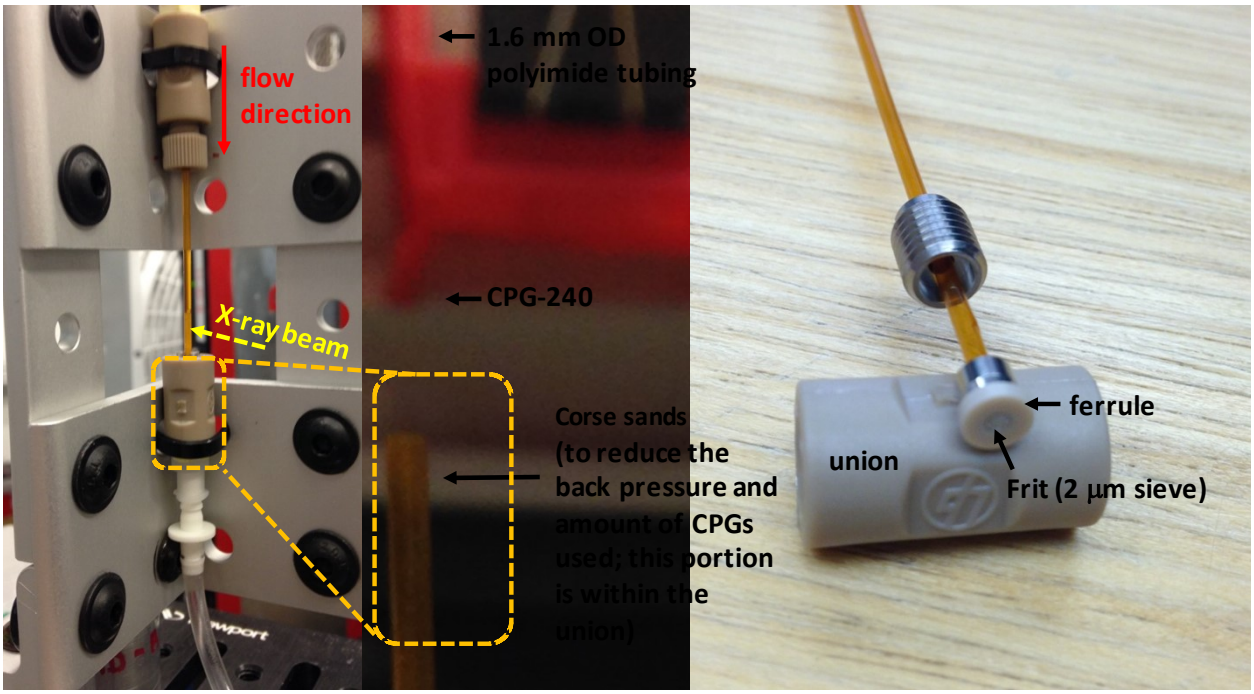

Figure S1. Photographs of the flow cell in various assembled states with labeled components.

2. X-ray Total Scattering Data Reduction

Data for an empty polyimide cell and several powder standards were collected for measurement background and calibration purposes. The software Fit2D[1] was used to calibrate the sample to detector distance and detector alignment with data from a CeO_2 standard, and integrate raw

scattering data into Q-space spectra, applying a mask and polarization correction. The normalized total scattering patterns, S(Q) were produced in PDFgetX2[2] by subtracting polyimide container scattering and applying standard corrections for the area detector setup.[3] Pair distribution function patterns, G(r), were produced utilizing a Q maximum of 21.5 $Å^{-1}$. As shown in Figure 1(c) of the ma text, the raw PDF data is dominated by the structural correlations of the CPG framework, corresponding to an amorphous SiO_2 network. Difference PDFs in Figure 1(b), created by subtracting the first 10 minutes of collected data from each dataset, exhibit both negative and positive pair-pair correlations. Negative correlations (arrows pointing down) coincide with the framework structure, and are removed from the final data by applying a background scale factor that minimizes intensity at the Si-O pair-pair correlation at ~1.64 Å. It is not possible to distinguish directly from the data whether the removal of silica (relative to the ACC phase) indicates CPG dissolution or simply a shifting amount of material in the x-ray beam throughout the experiment. To investigate this, we quantified the total dissolved silicon by inductively coupled plasma optical emission spectrometry (ICP-OES). The concentration oscillated around 4 ppm, which is below the detection limit of the PDF technique, suggesting the movement of CPG particles (with solution flow) is responsible for silica intensity variations. The utilized background scale factor and ICP results are shown in Figure 3(a). The overall result produced the series of normalized ΔG(r) shown in Figure 1(a) and used in quantitative analysis for the study.

3. X-ray Pair distribution Function Analysis

Least squares real-space modeling of the experimental G(r) was completed in PDFgui.[4] A Ni dataset was fit between 1 and 50 Å to refine the instrument specific parameters, Q_{damp} = 0.036 $Å^{-1}$ and Q_{broad} = 0.014 $Å^{-1}$, and these were held fixed during refinement. Literature models for crystalline calcite,[5] aragonite,[6] and monohydrocalcite[7] were used to fit reference sample data between 0.8 and 20 Å: parameters for lattice parameters, atomic positions (both constrained by symmetry), isotropic atomic displacement parameters (constrained by atom type), a scale factor, and a parameter to account for correlated motion effects at low real-space ranges were refined. The reference data, model fits, and refined parameters are provided in Figure S2 and Table S1. Parameter values for vaterite and ikaite were taken from literature models.[8,9]

For modeling the precipitate phase, the data was fit by holding the structural parameters for the crystalline forms fixed and varying only the applied scale factor and a spherical particle diameter parameter[11] that accounts for finite size effects.

4. Crystalline Reference Material Models

Data for samples of crystalline calcite, aragonite, and monohydrocalcite (all naturally occurring minerals), as well as a hydrated amorphous basic calcium carbonate[10] were collected for reference. Figure S2 displays the data and fits for crystalline standard materials applied in the analysis of precipitate data.

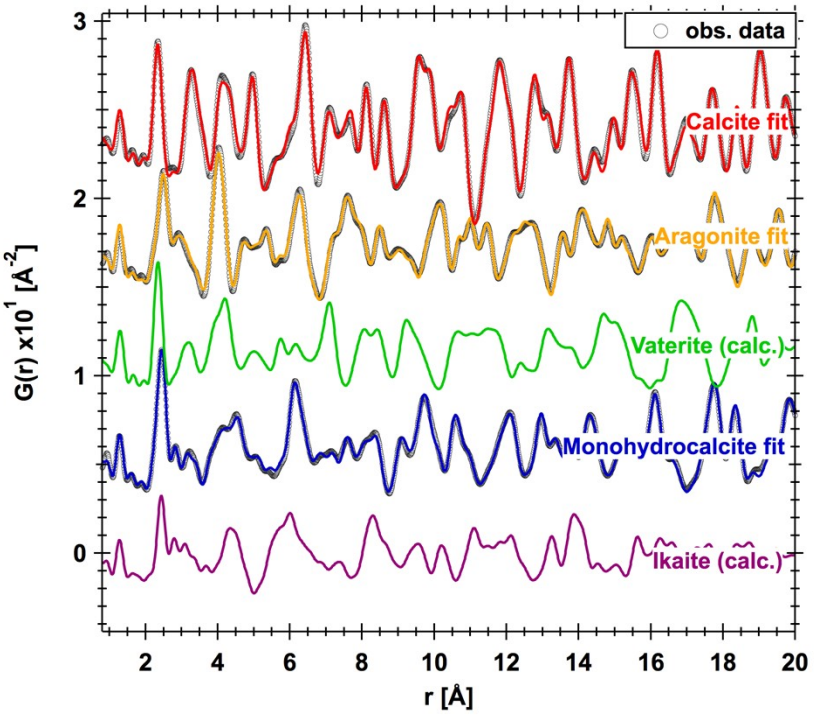

Figure S2. Data for crystalline standard materials (open grey circles) with fits to the data given as lines. A calculated data set for vaterite and ikaite, are also shown (green and purple lines, respectively).

Table S1. Refinement Summary for Calcite, Aragonite and Monohydrocalcite Reference Samples

	Calcite	**Aragonite**	**Monohydrocalcite**
space group	*R* -3 *c*	*P m c n*	*P* 3_1
scale factor	0.99(2)	1.01(2)	1.19(3)
δ_2	0.9(3)	1.2(2)	1.2(2)
sratio for r < *2.5* Å	0.64(4)	0.81(6)	0.62(6)
a (Å)	4.988(1)	4.958(3)	10.543(4)

b (Å)	4.988(1)	7.971(4)	10.543(4)
c (Å)	17.052(5)	5.739(4)	7.556(6)
Ca: U_{iso} (Å^2)	0.0057(2)	0.0056(4)	0.0054(4)
C: U_{iso} (Å^2)	0.0082(6)	0.008(2)	0.009(4)
O: U_{iso} (Å^2)	0.0162(6)	0.015(1)	0.012(1)
R_w	0.171	0.137	0.161

Table S1. (Continue)

	x	*y*	*z*
Calcite			
Ca	0.000	0.000	0.000
C	0.000	0.000	0.250
O	0.256(1)	0.000	0.250
Aragonite			
Ca	0.250	0.4152(5)	0.757(1)
C	0.250	0.761(2)	0.908(3)
O1	0.250	0.923(2)	0.906(3)
O2	0.475(2)	0.682(1)	0.911(2)

	x	*y*	*z*
Monohydrocalcite			
Ca1	0.182(6)	0.094(5)	0.333
Ca2	0.848(6)	0.426(5)	0.351(5)
Ca3	0.518(6)	0.753(6)	0.351(5)
C1	0.100(5)	0.176(6)	0.949(5)
C2	0.750(5)	0.514(6)	0.045(5)
C3	0.413(5)	0.840(6)	0.061(5)
O1	0.213(5)	0.242(5)	0.093(8)
O2	0.068(5)	0.054(5)	0.901(8)
O3	0.037(5)	0.250(5)	0.919(9)
O4	0.886(7)	0.588(5)	0.090(8)
O5	0.677(5)	0.403(5)	0.139(8)
O6	0.692(5)	0.572(5)	0.943(7)
O7	0.552(6)	0.911(5)	0.082(8)
O8	0.336(5)	0.723(6)	0.156(8)
O9	0.359(5)	0.902(5)	0.964(7)
Ow1	0.398(7)	0.204(5)	0.861(6)
Ow2	0.064(7)	0.542(6)	0.867(8)
Ow3	0.726(7)	0.881(5)	0.844(6)

5. Control Experiments in Bulk Solution and in Micropore Environment

5.1 Calcium carbonate growth solution

As noted in the main text, the composition of the growth solution was determined to have a $[Ca^{2+}]/[CO_3^{2-}]$ ratio of 90±1 and pH of 8.40±0.01 at 25 °C. The saturation index (SI) of this solution is ~0.75 with respective to calcite, ~0.60 with respective to aragonite, and ~0.17 with respective to vaterite. Although the growth solutions were apparently metastable, we however, do not observe any visible homogeneous precipitation in the solution reservoir after a whole day of experiments.

5.2 Growth of calcite in micropore environment

To investigate whether the change of pore sizes in the silica matrix can influence $CaCO_3$ heterogeneous growth behaviors, we performed another flow through experiment, where the nanoporous silica (CPG) matrix was replaced by SiO_2 glass microbeads to create micron-sized porous environments. The glass microbeads with average diameter of 90-150 μm (C-PGL-015, Corpuscular) were filled in the 1.1 mm OD polyimide tube (Cole-Parmer), using the same experimental setup shown in Figure S1. Calcium carbonate growth solution of the same composition used in the nanoporous silica (CPG) experiment was flowed through the microbead-filled column at a flow rate of 100 mL/h for 5 hours (identical conditions to the CPG experiment). In the microbead case, over time, we observed a drop off in the flow rate to about 85 mL/h, which suggests the precipitation of $CaCO_3$ mineral(s), eventually filling available micropores. Microbeads were sampled at the end of the flow-through experiments, and were mounted on a scanning electron microscope (SEM) aluminum stub for the subsequent morphological observations.

The morphology of precipitated $CaCO_3$ on the surface of glass microbeads were observed using a Hitachi S-4800 high resolution SEM. Samples were sputtered with a 5 nm gold coating layer to increase the conductivity. SEM images were taken in both secondary electron and back scattered (BSE) modes at an accelerating voltage of 5 kV and current of 20 μA. The SEM microscope is equipped with the Oxford's Ultim Max energy dispersive spectrometer (EDS) for elemental distribution analysis. EDS qualitative analysis and elemental mapping were performed at an accelerating voltage of 10 kV.

As shown in Figure S3, rhombohedral-shaped crystals are observed on the surface of glass microbeads. These crystals are found to be homogeneously distributed in both shapes and sizes (Figs. S3(b-c)), measured around 3-5 micron in scale. A few smaller rhombohedral nuclei with size of ~ 100-200 nm are also observed (Fig. S3(d)). Most of the crystals are observed to attach to the surface of the glass beads, suggesting heterogenous growth behaviors. In addition, the growth density over the glass beads surface is estimated around 10%. Figure S4 shows the results from EDS qualitative analysis, and indicates the $CaCO_3$ stoichiometry in the grown crystals. By combining morphological observations and chemical analysis, the precipitated carbonate mineral on the surface of glass beads is identified to be calcite.

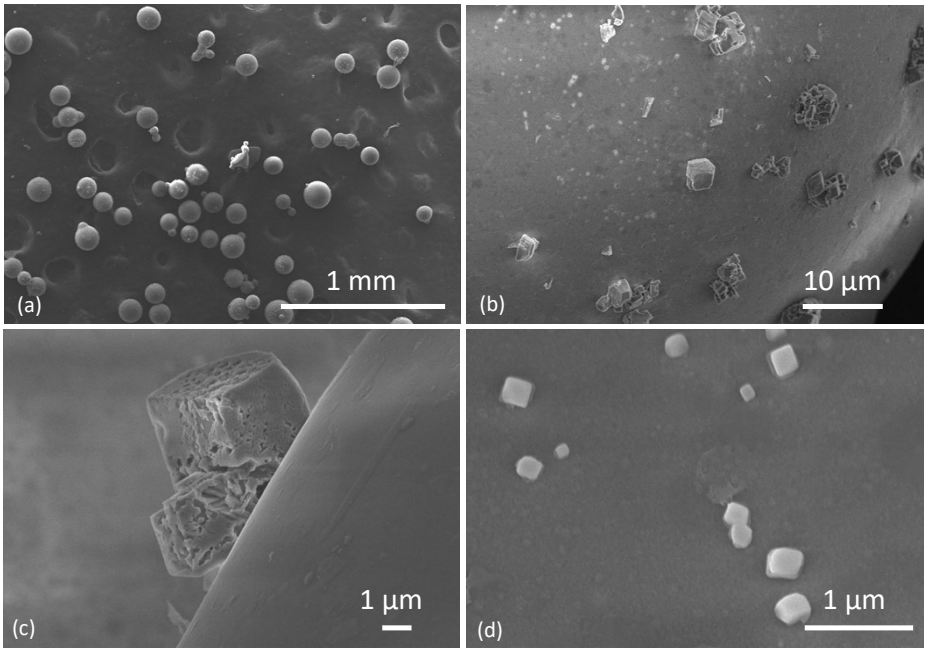

Figure S3. Secondary electron (SE) SEM images of calcite crystals grown (a-c) and nucleated (d) on the surface of glass microbeads after flowing calcium carbonate growth solution for five hours.

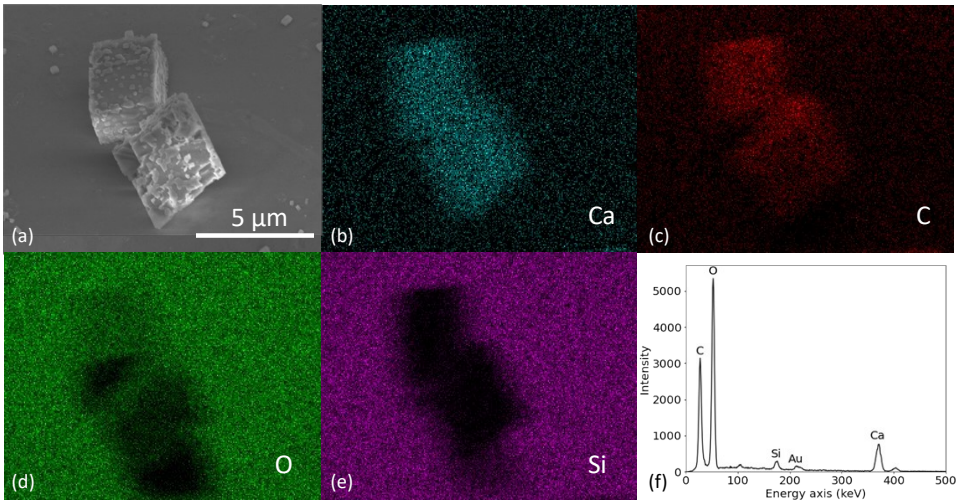

Figure S4. Scanning electron micrographs (a) of rhombohedral calcite crystals grown over the surface of glass beads. (b-e): Calcium (Ca), carbon (C), oxygen (O), and silicon (Si) EDS mapping of imaged area (a). (f) EDS spectrum of calcite crystals.

References

[1] Hammersley, A. P.; Svensson, S. O.; Hanfland, M.; Fitch, A. N.; Hausermann, D. *High Press. Res.* **1996**, 14, 235-248.
[2] Qiu, X.; Thompson, J. W.; Billinge, S. J. L. *J. Appl. Crystallogr*. **2004**, 37, 678-678.
[3] P. J. Chupas, X. Qiu, J. C. Hanson, P. L. Lee, C. P. Grey, S. J. Billinge, *J. Appl. Crystallogr*. **2003**, *36*, 1342-1347.
[4] Farrow, C. L.; Juhás, P.; Liu, J. W.; Bryndin, D.; Božin, E. S.; Bloch, J.; Proffen, Th.; Billinge, S. J. L. *J. Phys.: Condens. Mat*. **2007**, *19*, 335219.
[5] Graf, D L. *Am. Mineral.* **1961**, *46*, 1283-1316.
[6] de Villiers, J. P. R. *Am. Mineral.* **1971**, *56*, 758-767.
[7] Swainson, I. P. *Am. Mineral.* **2008**, *93*, 1014–1018.
[8] Demichelis, R.; Raiteri, P.; Gale, J.D.; Dovesi, R. *Cryst. Growth Des*., **2013**, *13*, 2247-2251.
[9] Hesse, K. F.; Kuppers, H.; Suess, E. *Z. Kristallogr.* **1983**, *163*, 227-231.
[10] Wang, H.-W.; Daemen, L.L.; Cheshire, M.C.; Kidder, M.K.; Stack, A.G.; Allard, L.F.; Neuefeind, J.C.; Olds, D.; Liu, J.; Page, K. *Chem. Commun.* **2017**, *53*, 2942-2945.